Distinguishing black holes from naked singularities through their accretion disk properties

Pankaj S. Joshi,[1,*] Daniele Malafarina,[2,1,†] and Ramesh Narayan[3,‡]

[1]*Tata Institute of Fundamental Research, Homi Bhabha Road, Colaba, Mumbai 400005, India*
[2]*Department of Physics, Fudan University, 220 Handan Road, Shanghai 200433, China*
[3]*Harvard-Smithsonian Center for Astrophysics, 60 Garden Street, Cambridge, MA 02138, USA*

We show that, in principle, a slowly evolving gravitationally collapsing perfect fluid cloud can asymptotically settle to a static spherically symmetric equilibrium configuration with a naked singularity at the center. We consider one such asymptotic final configuration with a finite outer radius, and construct a toy model in which it is matched to a Schwarzschild exterior geometry. We examine the properties of circular orbits in this model. We then investigate observational signatures of a thermal accretion disk in this spacetime, comparing them with the signatures expected for a disk around a black hole of the same mass. Several notable differences emerge. A disk around the naked singularity is much more luminous than one around an equivalent black hole. Also, the disk around the naked singularity has a spectrum with a high frequency power law segment that carries a major fraction of the total luminosity. Thus, at least some naked singularities can, in principle, be distinguished observationally from black holes of the same mass. We discuss possible implications of these results.

arXiv:1304.7331v2 [gr-qc] 6 May 2014

I. INTRODUCTION

The no hair theorems in black hole physics state that a black hole is completely characterized by three basic parameters, namely, its mass, angular momentum, and charge. Because of this extreme simplicity, the observational properties of a black hole are determined uniquely by these three intrinsic parameters plus a few details of the surrounding environment.

There is compelling observational evidence that many compact objects exist in the universe, and there are indications that some of these might have horizons [1]. However, there is as yet no direct proof that any of these objects is necessarily a black hole. The dynamical equations describing collapse in general relativity do not imply that the final endstate of gravitational collapse of a massive matter cloud has to be a black hole (see [2]); other possibilities are also allowed. In the case of a continual collapse, general relativity predicts that a spacetime singularity must form as the endstate of collapse. However, recent collapse studies show that, depending on the initial conditions from which the collapse evolves, trapped surfaces form either early or late during the collapse. Correspondingly, the final singularity may either be covered, giving a black hole, or may be visible as a naked singularity. If astrophysical objects of the latter kind hypothetically form in nature, it is important to be able to distinguish them from their black hole counterparts through observational signatures.

General relativity has never been tested in the very strong field regime, and very little is known about how matter behaves towards the end of the gravitational collapse of a massive star, when extremely large densities are reached and quantum effects possibly become relevant. Over the years, it has often been suggested that some exotic stable state of matter might occur below the neutron degeneracy threshold, allowing for the existence of quark stars, or boson stars, or even more exotic astrophysical objects (see for example [3]).

At present we cannot rule out the possibility that such compact objects do exist. On the other hand, the densities and sizes of compact objects in the universe vary enormously, depending on their mass. While a stellar mass quark star could have a density greater than that of a neutron star, a supermassive compact object at the center of a galaxy might have a density comparable to that of ordinary terrestrial matter. This means that it is difficult to come up with a single paradigm for all compact objects by simply modifying the equation of state of matter. Also, the processes that lead to the formation of stellar mass compact objects are different from those leading to supermassive objects. For one thing, time scales are very different. Stellar mass compact objects form in a matter of seconds, when the core of a massive dying star implodes under its own gravity. We know little about the physical processes that lead to the formation of supermassive compact objects, but whatever it is, it doubtless operates far more slowly than in the stellar-mass case.

In our view it is important to study viable theoretical models that, under reasonable physical conditions, lead to the formation of different kinds of compact objects, and to investigate the properties of these different end states. In recent times, much attention has been devoted to the observational properties of spacetimes that describe very compact objects or singularities where no horizon is present [4]. Many valid solutions of Einstein field equations exist which describe spacetimes that are not black holes. These are either vacuum solutions with naked singularities or collapse solutions in the presence of matter. Naked

*Electronic address: psj@tifr.res.in
†Electronic address: daniele@fudan.edu.cn
‡Electronic address: rnarayan@cfa.harvard.edu

singularity models include the Reissner-Nordstrom, Kerr and Kerr-Newman geometries with a range of parameter values that differentiate the black hole and naked singularity regimes. Collapse models include dust collapse, models with perfect fluids and those with other equations of state [2].

Note further that the classical event horizon structure of the Kerr metric can be altered in many ways. One way is by over-spinning the Kerr black hole in order to obtain a naked singularity [5]. Another is by introducing deformations or scalar fields to alter the spacetime and thus expose a naked singularity [6]. Although the physical viability of some of these examples is not clear, the fact remains that classical general relativity allows for the formation of naked singularities in a variety of situations. If singular solutions represent a breakdown of the theory in the regime of strong gravity, then a study of some of these models might provide clues to new physics. For example, string theory or quantum gravity corrections can remove the Kerr singularity, leaving open the possibility of non singular superspinning solutions [7].

In a recent paper [8], the present authors showed that equilibrium configurations describing an extended compact object can in principle be obtained from gravitational collapse. The models we described correspond to a slowly evolving collapsing cloud which settles asymptotically to a static final configuration that is either regular or has a naked singularity at the center. In this context, a naked singularity must be understood as a region of arbitrarily large density that is approached as comoving time goes to arbitrarily large values. We briefly examined the properties of accretion disks around the naked singularity solutions. There were significant physical differences compared to disks around black holes, and it followed that there could be astrophysical signatures that could distinguish black holes from naked singularities.

In the above previous work, we considered the case of purely tangential pressure and vanishing radial pressure. Are the solutions we obtained a consequence of this extreme simplification, or are they representative of a generic class of solutions that survive even for more reasonable equations of state? We answer this question here at least partly by exploring gravitational collapse of perfect fluid objects with an isotropic pressure. Even in this more realistic case, we find that objects with either regular interiors or naked singularities form readily as a result of gravitational collapse. We explore the similarities and differences between these new solutions and the earlier solutions which had purely tangential pressure.

Our main purpose in the present paper is to investigate whether the naked singularity models derived here and in our previous work can be observationally distinguished from black holes of the same mass. We therefore take a further step in this direction by calculating the spectral energy distributions of putative accretion disks. We show that important differences exist in the physical properties of accretion disks around naked singularities compared to those around black holes, which may help us distinguish black holes from naked singularities through observations of astrophysical objects. Although the toy models considered here are unlikely to be realized physically, some general features of these objects are revealed by our analysis and show that naked singularities could be observationally distinguished from black holes.

The structure of the paper is as follows: In section II we describe a procedure by which a static perfect fluid object with a Schwarzschild exterior metric can be obtained via gravitational collapse from regular initial conditions. In section III, we use the above procedure to obtain a toy model of a static final configuration with a naked singularity at the center. We then describe the properties of accretion disks in this toy spacetime and compare these models to disks around a Schwarzschild black hole of the same mass. We also briefly discuss other density profiles of astrophysical interest that could be studied within the same framework. In the final section IV, we discuss possible applications to astrophysical observations.

II. GRAVITATIONAL COLLAPSE

Spherical collapse in general relativity can be described by a dynamical spacetime metric of the form

$$ds^2 = -e^{2\nu}dt^2 + \frac{R'^2}{G}dr^2 + R^2 d\Omega^2 \ , \tag{1}$$

where ν, R and G are functions of the comoving coordinates t and r. For the perfect fluid case, the energy-momentum tensor is given by $T^0_0 = \epsilon,\ T^1_1 = T^2_2 = T^3_3 = p$. The Einstein equations then take the form

$$p = -\frac{\dot{F}}{R^2\dot{R}} \ , \tag{2}$$

$$\epsilon = \frac{F'}{R^2 R'} \ , \tag{3}$$

$$\nu' = -\frac{p'}{\epsilon + p} \ , \tag{4}$$

$$\dot{G} = 2\frac{\nu'}{R'}\dot{R}G \ , \tag{5}$$

where $(')$ denotes a derivative with respect to comoving radius r and $(\dot{})$ denotes a derivative with respect to time t in the (r,t) representation. The function F, called the Misner-Sharp mass, describes the amount of matter enclosed within the shell labeled

by r at the time t, and is given by

$$F = R(1 - G + e^{-2\nu}\dot{R}^2) \ . \tag{6}$$

Equations (2)–(6) give five relations among the six unknown functions $p(r,t)$, $\epsilon(r,t)$, $\nu(r,t)$, $G(r,t)$, $F(r,t)$ and $R(r,t)$. We thus have the freedom to specify one free function. An assumed equation of state relating pressure to energy density during the evolution of the system would fix this remaining freedom and give a closed set of equations. It could happen, however, that this approach leads to an analytically intractable problem. Moreover, we do not know if the collapsing matter will have the same unchanged equation of state as it evolves to higher and higher densities as the collapse progresses. There is in fact no astrophysical or mathematical requirement that the equation of state must be fixed as the collapse evolves in time. We therefore prefer here instead to choose the functional form of $F(r,t)$, which corresponds implicitly to fixing the equation of state, which could however change with time and space coordinates. We choose a scenario such that we approximate some standard equation of state at early times, switching to some other, possibly exotic, kind of matter at later times.

We use the scaling degree of freedom in the definition of R to fix the initial condition $R(r,t_i) = r$, where t_i is the initial time. To describe collapse we require $\dot{R} < 0$, which guarantees that R decreases monotonically with respect to t. Hence, we may change coordinates from (r,t) to (r,R), thus in effect considering $t = t(r,R)$. Correspondingly, we can view the original function $F(r,t)$ as a function of r and R and write $F = F(r,R)$. In the following, we use $(,r)$ to denote a derivative with respect to r in the (r,R) representation, i.e.,

$$F' = F_{,r} + F_{,R}R'. \tag{7}$$

The total mass of the system is not conserved during collapse, unless one requires the further condition that $F(r_b,t) = \mathrm{const}$, where r_b corresponds to the boundary of the system. Therefore, we cannot in general match a collapse solution to an exterior Schwarzschild metric. However, matching to a generalized Vaidya spacetime at the boundary $R_b(t) = R(r_b,t)$ is always possible [9].

The procedure to solve the above system of Einstein equations is the following. We choose the free function $F(r,R)$ globally and use equations (2) and (3) to obtain $p(r,R(r,t))$ and $\epsilon(r,R(r,t))$ as functions of r, R and its derivatives. We then integrate equation (4) to obtain ν,

$$\nu(r,R) = -\int_0^r \frac{p'}{\epsilon + p} d\tilde{r}, \tag{8}$$

and integrate equation (5) to obtain G,

$$G(r,R) = b(r)e^{2\int_r^R \frac{\nu'}{R'}d\tilde{R}}. \tag{9}$$

The free function $b(r)$ results from the integral in equation (9); it is related to the velocity profile in the collapsing cloud. The integral in equation (8) again gives a free function of t, but this can be absorbed via a redefinition of the time coordinate. Once we have $\nu(r,R)$ and $G(r,R)$ as functions of r, R and its derivatives, we can integrate the Misner-Sharp mass equation (6) that becomes a differential equation involving R and its derivatives. We can write it in the form

$$t_{,R} = -\frac{e^{-\nu}}{\sqrt{\frac{F}{R} + G - 1}}, \tag{10}$$

and its integration gives $t(r,R)$, or equivalently $R(r,t)$ thus solving the system.

Substituting equations (8) and (9) in equation (1), the metric of the collapsing spacetime takes the form

$$ds^2 = -e^{-2\int_0^r \frac{p'}{\epsilon+p}d\tilde{r}}dt^2 + \frac{R'^2}{b(r)e^{2\int_r^R \frac{\nu'}{R'}d\tilde{R}}}dr^2 + R^2 d\Omega^2 \ . \tag{11}$$

It may not always be possible to fully integrate the system of Einstein equations globally. However, this is not always needed, because by considering the behaviour of the functions involved, it is often possible to extract useful information about collapse and to integrate the solution at least in a neighborhood close to the center.

Typically some restrictions are required in order for the collapse model to be considered physically viable. They are:

1. Absence of shell crossing singularities, which arise from a breakdown of the coordinate system at locations where collapsing shells intersect. This requirement implies $R' > 0$. We note in this connection that there is always a neighborhood of the central line $r = 0$ of the collapsing cloud which contains no shell-crossing singularities throughout the collapse evolution [10].

2. Energy conditions, of which the usual minimal requirement is the weak energy condition, viz., positivity of the energy density ($\epsilon > 0$) and of the sum of density and pressure ($\epsilon + p > 0$). This requires $F'(r, R) > 0$ and $F_{,r}(r, R) > 0$.

3. Regularity at the center during collapse before the formation of the singularity. This includes the requirements that forces and pressure gradients vanish at the center and that the energy density has no cusps at $r = 0$. The corresponding requirements are $F(r, R) \simeq r^3 m(r, R)$ near $r = 0$, $m'(0, R) = 0$ and $p'(0, R) = 0$.

4. Absence of trapped surfaces at the initial time. This last requirement is given by positivity of $[1 - (F/R)]_{t=t_i}$ and translates to $\dot{R}^2_{t=t_i} < \left(e^{2\nu} G\right)_{t=t_i}$.

Our aim now is to construct a dynamical collapse evolution such that the pressure eventually balances gravitational attraction and the collapsing object settles into a static configuration. Such a scenario is of course not always possible in gravitational collapse of a massive matter cloud, and there are matter configurations that can only collapse indefinitely without achieveing any possible equilibrium. Such is the case of collapse of a pressureless dust cloud [11], or similar systems where pressure is very insignificant. Another possibility in collapse is that the cloud bounces back after reaching a minimum radius. Typically, since we begin with a collapsing configuration, for each shell labeled by the comoving radius r, three different behaviours are possible:

1. Collapse: $\dot{R} < 0$. If $\dot{R}$ is negative at all times the shell will collapses to a central singularity.

2. Bounce: $\dot{R} = 0$ at a certain time, with $\ddot{R} > 0$ at this time. The shell bounces back and re-expands.

3. Equilibrium configuration: $\dot{R} = \ddot{R} = 0$. Here the collapse slows down and the shell achieves a static configuration.

Shells that achieve an equilibrium configuration in a certain sense mark the separation between the region that collapses indefinitely and the region that eventually bounces back [12]. Both collapse and bounce would occur typically very rapidly, on a dynamical time scale which is proportional to the mass. Even in the case of supermassive compact objects, this time is much shorter than other typical time scales.

It would appear that all three possibilities above represent generic behavior during gravitational collapse, depending on the masses and velocities of the collapsing shells and the physical scenario involved in collapse. For example, for a very massive star, an indefinite collapse would seem inevitable if the star cannot shed away enough of its mass in a very short collapse time scale to achieve any possible equilibrium. On the other hand, for a much larger mass scale such as galactic or yet larger scales, the collapse could proceed much more slowly and even arrive at an equilibrium to form a stable massive object. It is well known of course that gravitational collapse plays a key role in the formation of large scale structures in the universe. In many such cases, an evolving collapse would slow down, eventually to form a stable massive object. In such cases, scenarios such as the one considered here could be relevant.

We note that in order to achieve an equilibrium object as the endstate of collapse or in order to have a useful quasi-equilibrium configuration, it is necessary that each collapsing shell in the cloud must individually achieve the condition $\dot{R} = \ddot{R} = 0$. Such an object can be well approximated by a static configuration. The equation of motion (6) can be written in terms of R, for any fixed comoving radius r, in the form of an effective potential:

$$V(r, R) = -\dot{R}^2 = -e^{2\nu} \left(\frac{F}{R} + G - 1 \right) . \tag{12}$$

We already know that no static configuration is possible for the pressureless (dust) case, where V is negative at all times. When there is pressure, it is still possible for V to be negative at all times, giving continued collapse. However, other possibilities are also allowed since at any given time t each shell r can be either collapsing, expanding or still giving rise to a wide array of scenarios. We shall consider here the simple but very common case where V, as a function of R for fixed r, is a polynomial of second order in R. We see that one generic possibility in this case is that V has two distinct zeroes. In this case, the shell will bounce at a finite radius and re-expand. Another possibility is that the two zeroes of V coincide (namely V has one root of double multiplicity) corresponding to an extremum at $V = 0$. In this case, the shell will coast ever more slowly towards the radius corresponding to $V = 0$ and will halt without bouncing having reached such radius with zero velocity and zero acceleration as t goes to infinity. A global static configuration for this form of the potential is then achieved only if each shell satisfies the condition that it has one double root. It is not difficult to see that the velocity of the cloud during collapse is always non-zero and therefore such an equilibrium configuration can be achieved only in a limiting sense, as the comoving time t goes to infinity (for a more detailed discussion on the condition leading to equilibrium see [8]). For more general forms of the potential the allowed regions of dynamics for the shell and its behaviour are decided by the multiplicity of the roots of V.

The condition that the spacetime evolves towards an equilibrium configuration is thus

$$\dot{R} = \ddot{R} = 0, \tag{13}$$

which is equivalent to

$$V = V_{,R} = 0. \tag{14}$$

From equation (12) we find

$$V_{,R} = e^{2\nu}\left(\frac{F}{R^2} - \frac{F_{,R}}{R} + G_{,R}\right) - 2\nu_{,R}e^{2\nu}\left(\frac{F}{R} + G - 1\right) \ . \tag{15}$$

The system achieves an equilibrium configuration if the solution of the equation of motion (10), given by $R(r,t)$, tends asymptotically to an equilibrium solution $R_e(r)$ such that the conditions given in equations (13) or (14) are satisfied. Therefore, in order to have

$$R(r,t) \xrightarrow[t\to\infty]{} R_e(r), \tag{16}$$

we must choose the free function $F(r,R)$ in the dynamical collapse scenario such that the quantities F, ν, G tend to their respective equilibrium limits:

$$F(r,R) \ \rightarrow \ F_e(r) = F(r,R_e(r)), \tag{17}$$
$$\nu(r,R) \ \rightarrow \ \nu_e(r) = \nu(r,R_e(r)), \tag{18}$$
$$G(r,R) \ \rightarrow \ G_e(r) = G(r,R_e(r)). \tag{19}$$

Imposing the conditions (14), we thus obtain two equations which fix the behaviour of G and $G_{,R}$ at equilibrium:

$$G_e(r) \ = \ 1 - \frac{F_e}{R_e} \ , \tag{20}$$
$$(G_{,R})_e \ = \ G_{,R}(r,R_e(r)) = \frac{F_e}{R_e^2} - \frac{(F_{,R})_e}{R_e} \ , \tag{21}$$

where the velocity profile $b(r)$ in equation (9) has been absorbed into $G_e(r)$.

Note that at equilibrium the area radius R becomes a monotonic increasing function of r. Therefore if we define the new radial coordinate ρ at equilibrium as

$$\rho \equiv R_e(r), \tag{22}$$

we can rewrite the functions at equilibrium as

$$F_e(r) \ = \ \mathrm{F}(\rho), \tag{23}$$
$$\nu_e(r) \ = \ \phi(\rho), \tag{24}$$
$$G_e(r) \ = \ \mathrm{G}(\rho) = 1 - \frac{\mathrm{F}}{\rho}. \tag{25}$$

Then, from equations (3) and (4), two of the Einstein equations for a static source become

$$\epsilon(\rho) \ = \ \frac{\mathrm{F}_{,\rho}}{\rho^2}, \tag{26}$$
$$p_{,\rho} \ = \ -(\epsilon + p)\phi_{,\rho}, \tag{27}$$

where $(,\rho)$ denotes a derivative with respect to the new static radial coordinate ρ. The second equation is the well known Tolman-Oppenheimer-Volkoff (TOV) equation. The third static Einstein equation, namely

$$p = \frac{2\phi_{,\rho}}{\rho}\mathrm{G}(\rho) - \frac{\mathrm{F}(\rho)}{\rho^3}, \tag{28}$$

is obtained from equation (2) by imposing the equilibrium condition and making use of equation (5) at equilibrium. The metric (11) at equilibrium then becomes the familiar static spherically symmetric spacetime,

$$ds^2 = -e^{2\phi}dt^2 + \frac{d\rho^2}{\mathrm{G}} + \rho^2 d\Omega^2, \qquad \rho \leq \rho_b \equiv R_e(r_b). \tag{29}$$

This interior metric is matched to a Schwarzschild vacuum exterior at the boundary $\rho_b = R_e(r_b)$. By matching $g_{\rho\rho}$ at the matching radius ρ_b and making use of equation (25), we see that the total gravitational mass M_T of the interior is given by

$$1 - \frac{2M_T}{\rho_b} = G(\rho_b) = 1 - \frac{F(\rho_b)}{\rho_b}. \tag{30}$$

Note that, in principle, the interior metric in equation (29) need not be regular at the center, as the eventual singularity is achieved as the result of collapse from regular initial data. A singularity at the center of the static final configuration is then interpreted as a region of arbitrarily high density that is achieved asymptotically as the comoving time t goes to arbitrarily large values. Therefore when considering static interiors with a singularity we are in fact approximating a slowly evolving configuration, where shells have typically very 'small' velocities and where the central region can reach very high densities.

Typically, for a static perfect fluid source of the Schwarzschild geometry, various conditions could be required in order to ensure physical reasonability [13]. Some of these are: the matter satisfies an energy condition, matching conditions with the exterior Schwarzschild geometry, vanishing of the pressure at the boundary, monotonic decrease of the energy density and pressure with increasing radius, sound speed within the cloud should be smaller than the speed of light. If the energy conditions are satisfied during collapse, they will be satisfied by the equilibrium configuration as well, i.e., the positivity of the energy density and sum of density and pressure at the origin follows from the same condition during collapse. Also, requiring only the weak energy condition allows the possibility of negative pressures either during the collapse phase or in the final equilibrium configuration.

Since we have required here the static configuration to evolve from regular initial data, we may omit the condition that the final state must be necessarily regular at the center. This leaves open the possibility that a central singularity might develop as the equilibrium is reached, where the singularity has to be understood in the sense explained above. Absence of trapped surfaces at the initial time ensures that, if a singularity develops, it will not be covered by a horizon [14]. In fact it can be shown that if trapped surfaces do form at a certain time as the cloud evolves, then the collapse cannot be halted and the whole cloud must collapse to a black hole or to a singularity where the first point of singularity is visible but the later portions of the singularity become covered in a black hole. We note that some of the above conditions, although desirable, may be neglected in special cases. Many interior solutions are available in the literature describing a static sphere of perfect fluid matching smoothly to a Schwarzschild exterior geometry (see [15] for a list of solutions or [16] for an algorithm to construct interior solutions). As discussed above, we can construct dynamically evolving collapse scenarios that lead asymptotically to the formation of such static configurations. If we are able to achieve a static configuration from collapse from regular initial data, and if we view a singularity as a region where density increases to arbitrarily high values, signaling a breakdown of the ability of general relativity to model the spacetime, we may then neglect the requirement of regularity at the center.

III. A TOY MODEL OF A STATIC SPHERICALLY SYMMETRIC PERFECT FLUID INTERIOR

In the following, we look for static interiors with a singularity at the origin. We wish to investigate the properties of such solutions and to establish whether such hypothetical naked singularity objects could in principle be distinguished in terms of observational signatures from black hole counter-parts of the same mass.

We start with the most general static spherically symmetric metric written in the form given in equation (29). As we have seen, the perfect fluid source Einstein equations give

$$\epsilon = \frac{\mathrm{F}_{,\rho}}{\rho^2}, \tag{31}$$

$$p = \frac{2\phi_{,\rho}}{\rho}\left[1 - \frac{\mathrm{F}(\rho)}{\rho}\right] - \frac{\mathrm{F}(\rho)}{\rho^3}, \tag{32}$$

$$p_{,\rho} = -(\epsilon + p)\phi_{,\rho}, \tag{33}$$

where we have absorbed the factor 4π into the definition of ϵ and p, and defined $\mathrm{F}_{,\rho} = d\mathrm{F}/d\rho$. The third (Tolman-Oppenheimer-Volkoff) equation, combined with the second equation, gives

$$p_{,\rho} = -(\epsilon + p)\frac{\left[p\rho^3 + \mathrm{F}(\rho)\right]}{2\rho\left[\rho - \mathrm{F}(\rho)\right]}. \tag{34}$$

Since the above system of Einstein equations consists of three equations with four unknowns, in order to close the system we can either specify an equation of state that relates p to ϵ or use the freedom to choose arbitrarily one of the other functions [17]. As discussed earlier, we opt for the latter approach and specify the form of the mass profile $\mathrm{F}(\rho)$, which describes the final mass distribution obtained from collapse. Once we specify F, equation (34) reduces to a first-order ordinary differential equation, which we can solve.

We follow the same procedure that we used in the pure tangential pressure case [8] and obtain a solution of the form

$$\frac{\mathrm{F}(\rho)}{\rho} = M_0 = \mathrm{const}, \qquad \rho \leq \rho_b. \tag{35}$$

By equation (30), this solution corresponds to a total mass M_T given by

$$2M_T = \mathrm{F}(\rho_b) = M_0 \rho_b. \tag{36}$$

Hence, to avoid a horizon, we require $M_0 < 1$. Solving the first Einstein equation (31), the energy density becomes

$$\epsilon = \frac{M_0}{\rho^2}, \tag{37}$$

which clearly diverges as $\rho \to 0$, indicating the presence of a strong curvature singularity at the center.

The TOV equation (34) now becomes

$$p_{,\rho} = -\frac{(\epsilon + p)^2 \rho}{2(1 - M_0)} = -\frac{(M_0 + p\rho^2)^2}{2\rho^3(1 - M_0)}, \tag{38}$$

which can be integrated by defining the auxiliary parameter

$$\lambda = \sqrt{\frac{1 - 2M_0}{1 - M_0}}, \qquad M_0 = \frac{1 - \lambda^2}{2 - \lambda^2}. \tag{39}$$

Clearly, we require $\lambda \in [0, 1)$, or equivalently $M_0 < 1/2$ (for values of $M_0 > 1/2$ similar considerations apply with $\lambda = \sqrt{-(1 - 2M_0)/(1 - M_0)}$ but we do not consider this case here). In terms of λ, the solution of equation (38) can be written as

$$p = \frac{1}{2 - \lambda^2} \frac{1}{\rho^2} \left[\frac{(1 - \lambda)^2 A - (1 + \lambda)^2 B \rho^{2\lambda}}{A - B\rho^{2\lambda}} \right], \tag{40}$$

where A and B are arbitrary integration constants. Then, solving the remaining Einstein equation gives

$$e^{2\phi} = (A\rho^{1-\lambda} - B\rho^{1+\lambda})^2. \tag{41}$$

This solution, among other similar interior static solutions, was first investigated by Tolman in 1939 for a specific choice of λ [18]. The energy density of the solution may be rewritten as

$$\epsilon = \left(\frac{1 - \lambda^2}{2 - \lambda^2} \right) \frac{1}{\rho^2}. \tag{42}$$

The existence of a strong curvature singularity at the center can be confirmed by an analysis of the Kretschmann scalar K near $\rho = 0$, which gives

$$K = \frac{16Q^4(1 - \lambda^2)^2 + \rho^4(Q_{,\rho}^2 - 2QQ_{,\rho\rho})^2 + 8\rho^2 Q^2 Q_{,\rho}^2}{4\rho^4 Q^4 (2 - \lambda^2)^2}, \qquad Q(\rho) = e^{2\phi(\rho)}, \tag{43}$$

which is clearly singular in the limit $\rho \to 0$.

The static metric of the above solution takes the form

$$ds^2 = -(A\rho^{1-\lambda} - B\rho^{1+\lambda})^2 dt^2 + (2 - \lambda^2) d\rho^2 + \rho^2 d\Omega^2, \qquad \rho \leq \rho_b. \tag{44}$$

It is matched at the boundary ρ_b to a vacuum Schwarzschild spacetime with total mass M_T. Since $g_{\rho\rho}$ in the interior is a constant, the matching will not in general be smooth, though it will be continuous. From the matching conditions for $g_{\rho\rho}$ and g_{tt} at the boundary we obtain,

$$\rho_b = \frac{2(2 - \lambda^2)}{(1 - \lambda^2)} M_T, \tag{45}$$

$$B\,\rho_b^{2\lambda} = A - \frac{\rho_b^{\lambda - 1}}{\sqrt{2 - \lambda^2}}. \tag{46}$$

For all values of $\lambda \in [0,1)$, the pressure is maximum at the center and decreases outwards, becoming zero at a finite radius ρ_p given by

$$\rho_p^{2\lambda} = \frac{A}{B}\frac{(1-\lambda)^2}{(1+\lambda)^2}. \tag{47}$$

Since we require the pressure to vanish at the boundary of the cloud, we obtain the further condition $\rho_b = \rho_p$, which, together with equation (46), fixes the two integration constants A and B:

$$A = \frac{(1+\lambda)^2\rho_b^{\lambda-1}}{4\lambda\sqrt{2-\lambda^2}}, \tag{48}$$

$$B = \frac{(1-\lambda)^2\rho_b^{-\lambda-1}}{4\lambda\sqrt{2-\lambda^2}}. \tag{49}$$

The sound speed inside the cloud is given by $c_s^2 = \partial p/\partial\epsilon$. We find

$$c_s^2 = \frac{p}{\epsilon} + \frac{4\lambda^2 ABr^{2\lambda}}{(1-\lambda^2)(A-Br^{2\lambda})^2}, \qquad \frac{p}{\epsilon} = \frac{A\frac{1-\lambda}{1+\lambda} - B\frac{1+\lambda}{1-\lambda}\rho^{2\lambda}}{A-B\rho^{2\lambda}}, \tag{50}$$

from which we see that $c_s(0) = (1-\lambda)(1+\lambda) < 1$, as required, and c_s decreases as the radius ρ goes from 0 to ρ_b. We may also rewrite the above relations in the form of an equation of state, $p = p(\epsilon)$,

$$p(\epsilon) = \epsilon\frac{A\left(\frac{1-\lambda}{1+\lambda}\right)\left(\frac{2-\lambda^2}{1-\lambda^2}\right)^{\lambda}\epsilon^{\lambda} - B\left(\frac{1+\lambda}{1-\lambda}\right)}{A\left(\frac{2-\lambda^2}{1-\lambda^2}\right)^{\lambda}\epsilon^{\lambda} - B}. \tag{51}$$

In the limit $\lambda \to 0$, corresponding to $M_0 \to 1/2$, we obtain the most compact member of the above family of solutions. It has an equation of state $p \approx \epsilon$ and hence sound speed $c_s \to 1$. Note, however, that at the outer boundary, $p \to 0$ but ϵ does not vanish, so the equation of state is not strictly isothermal. For this solution, the matching radius with the Schwarzschild exterior is at $\rho_b = 4M_T$, i.e., twice the Schwarzschild radius. In the case of pure tangential pressure, which we considered in our previous paper [8], we found physically meaningful solutions down to $\rho_b = 3M_T$, and even more compact solutions with exotic properties. This is one respect in which the perfect fluid model differs from the tangential pressure case.

For $\lambda = 1/2$, corresponding to $M_0 = 3/7$, we obtain an equation of state

$$p = \frac{\epsilon}{3}\left(1 - \frac{8B}{A\sqrt{\frac{7}{3}\epsilon} - B}\right), \tag{52}$$

which approaches the radiation equation of state $p = \epsilon/3$ as $\rho \to 0$. For this model, $\rho_b = (14/3)M_T$, i.e., the object is a little less compact than the model with $\lambda \to 0$.

Finally, the case $\lambda \to 1$, $M_0 \to 0$, corresponds to $\rho_b/M_T \to \infty$, and hence an infinitely large object. In this limit, our solution reduces to the classical Newtonian singular isothermal sphere solution. Correspondingly, $A \to 1$, $B \to 0$, and the metric in equation (44) reduces to the metric of flat space.

Considering next the energy conditions, it is easy to see that $M_0 > 0$ implies positivity of the energy density and pressure. The pressure decreases from its maximum value at the center to zero at the boundary. From

$$\epsilon + p = \frac{(1-\lambda)(1+\lambda)}{2-\lambda^2}\frac{1}{\rho^2}\left(1+\frac{p}{\epsilon}\right), \tag{53}$$

we see that the weak energy condition is satisfied throughout the interior of the cloud.

A. Properties of circular orbits

We wish to investigate basic observational properties of accretion disks orbiting in the above family of spacetimes. To this end, we study circular geodesics. Our assumption is that a test particle orbiting inside the "cloud" does not interact with the material of the cloud but merely feels its gravitational influence [34].

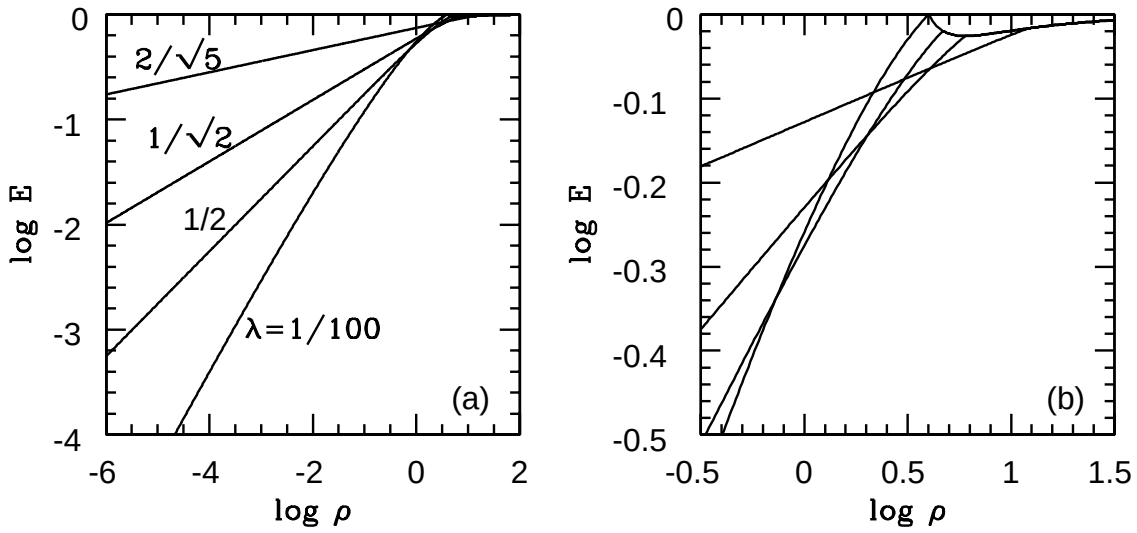


FIG. 1: (a) Energy per unit mass E of circular orbits as a function of radius ρ for four perfect fluid models of unit mass ($M_T = 1$). The parameter λ and the radius of the boundary ρ_b of the four models are, respectively: $(\lambda,\ \rho_b) = (1/100,\ 4.0002)$; $(1/2,\ 14/3)$; $(1/\sqrt{2},\ 6)$; $(2/\sqrt{5},\ 12)$. The curves are labeled by their values of λ. Each solution is matched to a Schwarzschild exterior at $\rho = \rho_b$. (b) Close up of the matching region between the perfect fluid interior and the Schwarzschild exterior. The models with $\lambda = 1/100$, 1/2, have ρ_b lying inside the innermost stable circular orbit $\rho_{\rm ISCO} = 6$ of the Schwarzschild spacetime. For these two solutions, E decreases between ρ_b and $\rho_{\rm ISCO}$, indicating a zone of unstable circular orbits.

Our perfect fluid model has five parameters, M_T, λ, ρ_b, A, B, and there are three matching conditions at the boundary $\rho = \rho_b$, viz., matching of g_{tt} and $g_{\rho\rho}$ with the exterior Schwarzschild metric and the condition $p(\rho_b) = 0$. Thus, we are free to choose two of the five parameters. For convenience, in the following we choose the total gravitational mass of the cloud M_T to be equal to unity. This still leaves one free parameter, which we choose to be λ. Once we pick a value of λ, the boundary radius ρ_b is given by equation (45), and the coefficients A and B are given by equations (48) and (49).

Given the spherical symmetry of the metric we can always choose the coordinate θ such that the geodesic under consideration lies in the equatorial plane ($\theta = \pi/2$). Time-like geodesics in this plane satisfy

$$-H(\rho)\left(\frac{dt}{d\tau}\right)^2 + (2-\lambda^2)\left(\frac{d\rho}{d\tau}\right)^2 + \rho^2\left(\frac{d\varphi}{d\tau}\right)^2 = -1, \tag{54}$$

where $H(\rho) = (A\rho^{1-\lambda} - B\rho^{1+\lambda})^2$.

From the two killing vectors, ζ^b, η^a, associated with time-translational symmetry and rotational symmetry, we can calculate two conserved quantities, the energy per unit mass, $E = g_{ab}\zeta^a u^b = e^{2\phi}dt/d\tau = Hdt/d\tau$, and the angular momentum per unit mass, $L = g_{ab}\eta^a u^b = \rho^2 d\varphi/d\tau$. For circular geodesics we must have $d\rho/d\tau = 0$. Therefore, we obtain

$$E^2 = \frac{2H^2}{2H - H_{,\rho}\rho}, \tag{55}$$

$$\frac{L^2}{\rho^2} = \frac{H_{,\rho}\rho}{2H - H_{,\rho}\rho}. \tag{56}$$

Figure 1 shows the variation of the energy per unit mass E with radius ρ for a selection of models corresponding to $\lambda = 1/100$, $1/2$, $1/\sqrt{2}$, $2/\sqrt{5}$. The boundaries of the four models are at (see eq. 45) $\rho_b = 4.0002, 14/3, 6$ and 12. In all the models, E goes to zero as $\rho \to 0$, with a power-law dependence: $E \sim \rho^{1-\lambda}$. At $\rho = \rho_b$, each model is matched to an exterior Schwarzschild spacetime with mass $M_T = 1$. Panel (b) in Figure 1 shows the matching region.

By construction, E is continuous across the matching boundary, but $dE/d\rho$ is not. Note in particular that the vacuum Schwarzschild spacetime has an innermost stable circular orbit (ISCO) at $\rho_{\rm ISCO} = 6$. For $\rho < \rho_{\rm ISCO}$, E increases with decreasing ρ, which is one of the consequences of the absence of stable orbits. The model with $\lambda = 2/\sqrt{5}$ has its boundary at $\rho_b = 12$ and hence has stable circular orbits all the way from large radii down to $\rho \to 0$. So too does the model with $\lambda = 1/\sqrt{2}$

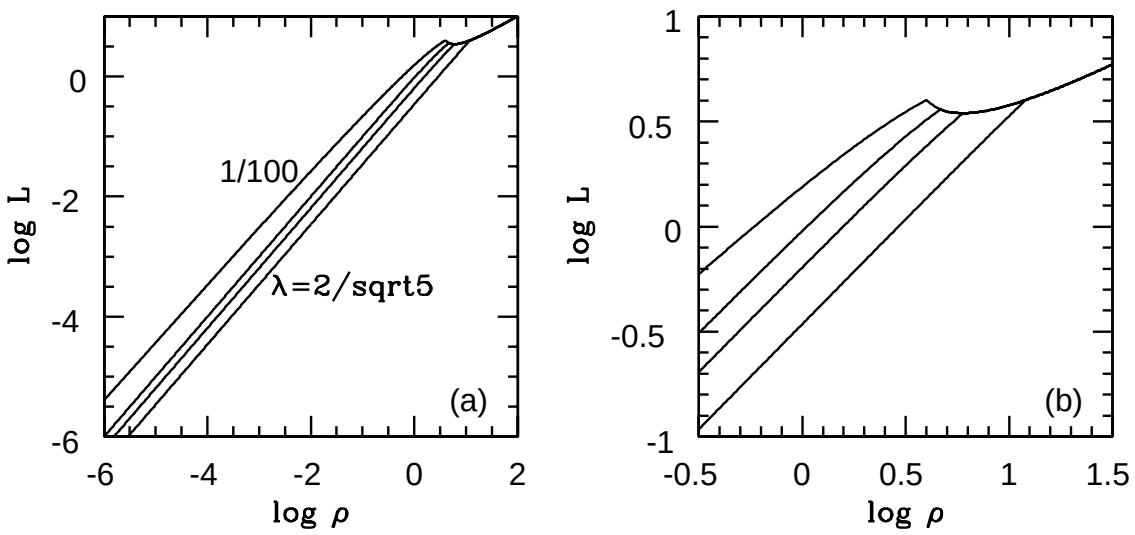


FIG. 2: (a) Angular momentum per unit mass L of circular orbits as a function of radius ρ for the same four perfect fluid models shown in Figure 1. The values of λ are: $1/100$, $1/2$, $1/\sqrt{2}$, $2/\sqrt{5}$ (the curves corresponding to the first and last solutions are labeled). (b) Close up of the matching region between the perfect fluid interior and the Schwarzschild exterior. Note, as in Figure 1, that the solutions with $\lambda = 1/100$, $1/2$ have L decreasing between ρ_b and $\rho_{\rm ISCO} = 6$. Circular orbits are unstable over this range of radius.

which has its matching radius at the ISCO, $\rho_b = \rho_{\rm ISCO}$. However, the other two models ($\lambda = 1/2, 1/100$) have $\rho_b < \rho_{\rm ISCO}$. Hence, these models have stable circular orbits inside ρ_b and outside $\rho_{\rm ISCO} = 6$, but no stable orbits in between.

Figure 2 shows analogous results for the angular momentum per unit mass L. Here, at small radii, $L \sim \rho$ for all the models. As in the case of E, the angular momentum matches continuously across the boundary $\rho = \rho_b$ to the external Schwarzschild solution. As panel (b) shows, the two models with $\lambda = 1/100$ and $1/2$ have $dL/d\rho < 0$ for a range of radii between ρ_b and $\rho_{\rm ISCO}$. This corresponds to the region with unstable circular orbits.

The angular velocity $\omega = d\phi/dt$ of particles on circular orbits is given by

$$\omega^2 = -\frac{g_{tt,\rho}}{g_{\phi\phi,\rho}} = \frac{H_{,\rho}}{2\rho}. \tag{57}$$

This quantity scales as $\omega \sim \rho^{-\lambda}$ as $\rho \to 0$. Figure 3 shows a plot of ω vs ρ for the same four models as before.

B. Properties of accretion disks

Gas in an accretion disk loses angular momentum as a result of viscosity and moves steadily inwards along a sequence of nearly circular orbits. Using just the properties of circular geodesics, and without needing to know the detailed properties of the viscous stress, it is possible to calculate the radiative flux emitted at each radius in the disk [20].

Since in our model both E and L tend to zero as ρ goes to zero, no energy or angular momentum is added to the central singularity by the gas in the accretion disk. The central singularity may be considered to be 'stable' in this sense. Indeed, since $E \to 0$, all the mass energy of the accreting gas is converted to radiation and returned to infinity, i.e., the net radiative luminosity as measured at infinity satisfies $\mathcal{L}_\infty = \dot{m}c^2$, where $\dot{m}$ is the rate at which rest mass is accreted. Accretion disks around our model naked singularity solutions are thus perfect engines that convert mass into energy with 100% efficiency.

From the behaviour of E and L of circular geodesics (Figs. 1 and 2), we can distinguish two different regimes of accretion, depending on the value of λ:

- For $\lambda \in [1/\sqrt{2}, 1)$, corresponding to $\rho_b \in [6M_T, +\infty)$, particles in the accretion disk follow circular geodesics of the Schwarzschild exterior until they reach the matching radius ρ_b at the outer edge of the cloud. Inside the cloud, the particles switch smoothly and continuously to the circular geodesics of the interior solution. Thus, the accretion disk extends without any break from arbitrarily large radii down to the singularity $\rho \to 0$.

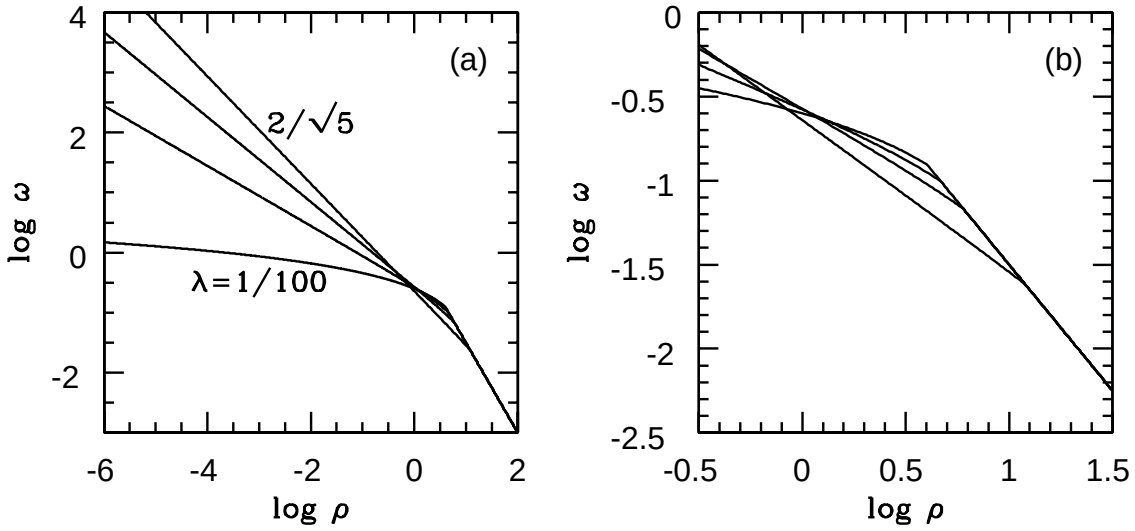


FIG. 3: (a) Angular velocity ω of circular orbits as a function of radius ρ for the same four perfect fluid models shown in Figure 1. The values of λ are: $1/100$, $1/2$, $1/\sqrt{2}$, $2/\sqrt{5}$ (the curves corresponding to the first and last solutions are labeled). (b) Close up of the matching region between the perfect fluid interior and the Schwarzschild exterior.

- For $\lambda \in (0, 1/\sqrt{2})$, corresponding to $\rho_b \in (4M_T, 6M_T)$, particles reach the ISCO of the exterior Schwarzschild spacetime at $\rho_{\rm ISCO} = 6$. Inside this radius no stable circular orbits are allowed, so the gas in the disk plunges with constant $E = E_{\rm ISCO}$ and $L = L_{\rm ISCO}$ until it crosses the boundary of the cloud at ρ_b. Inside the cloud, circular geodesics are allowed again. The gas penetrates into the cloud until it reaches a radius ρ_L at which the specific angular momentum of a local circular geodesic L is equal to $L_{\rm ISCO}$. At this radius, the gas settles into a stable circular orbit and radiates away any excess energy. Further evolution than proceeds in the standard fashion, with the gas steadily moving to smaller radii until $\rho \to 0$. The accretion disk is thus divided into two parts, one in the vacuum exterior over radii $\rho \geq \rho_{\rm ISCO}$ and the other inside the cloud over radii $\rho \leq \rho_L$.

In the following, we focus on models belonging to the first regime, where we have a continuous disk extending with no break from large radius down to the singularity. Specifically, we consider models with $\lambda = 1/\sqrt{2}, 2/\sqrt{5}$, which have matching boundaries at $\rho_b = 6, 12$, respectively. The radiative properties of accretion disks in these spacetimes may be calculated using the relations given in [20]. In the local frame of the accreting fluid, the radiative flux emitted by the disk (which is the energy per unit area per unit time) is given by

$$\mathcal{F}(\rho) = -\frac{\dot{m}}{4\pi\sqrt{-g}}\frac{\omega_{,\rho}}{(E-\omega L)^2}\int_{\rho_{in}}^{\rho}(E-\omega L)L_{,\tilde{\rho}}d\tilde{\rho}\ , \tag{58}$$

where $\dot{m}$ is the rest mass accretion rate, assumed to be constant, $\rho_{\rm in}$ is the radius of the inner edge of the accretion disk, which is zero for our singular cloud models, and g is the determinant of the metric of the three-sub-space (t, ρ, ϕ),

$$g(\rho) = -(2-\lambda^2)\rho^2 H(\rho). \tag{59}$$

The solid curves in Figure 4(a) show the variation of $\mathcal{F}(\rho)$ vs ρ for the two chosen models. The flux diverges steeply as the gas approaches the center: $\mathcal{F} \sim \rho^{-(3-\lambda)}$. This is not surprising, considering that the cloud is singular in this limit. Perhaps more surprising is the discontinuity in the flux at the boundary between the cloud and the external vacuum metric, as seen clearly in Figure 4(b). While all the quantities E, L, ω, g which are present in equation (58) are continuous across the boundary, the derivative $\omega_{,\rho}$ is not. The discontinuity in $\omega_{,\rho}$ causes the jump in F as ρ crosses ρ_b. The dotted lines in the two panels correspond to an accretion disk around a Schwarzschild black hole. In this case, the inner edge of the disk is at $\rho_{\rm in} = \rho_{\rm ISCO} = 6$, and the flux cuts off at this radius.

We note of course that the flux $\mathcal{F}$ is a local quantity measured in the frame of the fluid and is not directly observable. A more useful quantity is the luminosity $\mathcal{L}_\infty$ (energy per unit time) that reaches an observer at infinity. The differential of $\mathcal{L}_\infty$ with

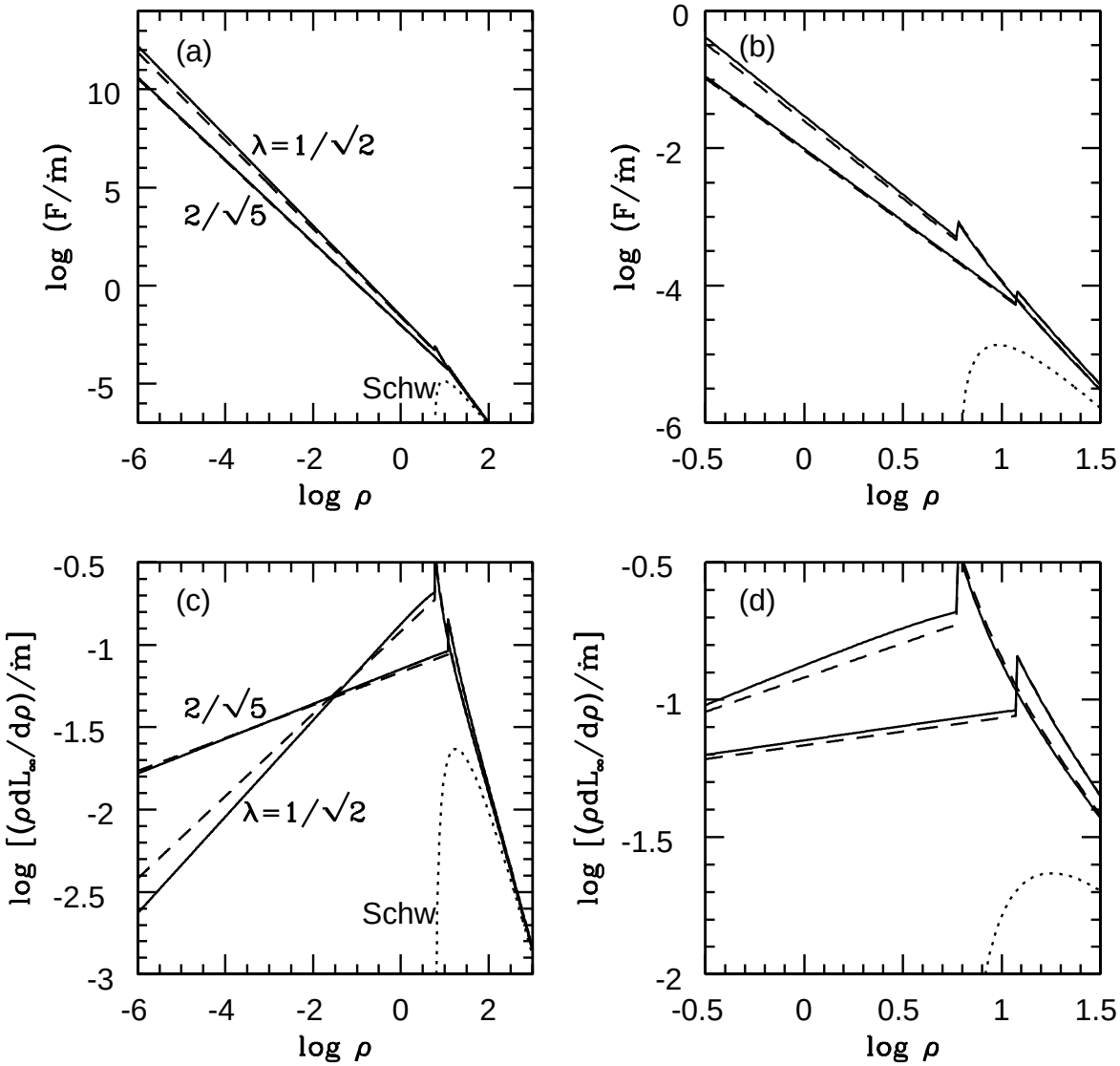


FIG. 4: (a) The two solid lines show the variation of the radiative flux $\mathcal{F}$ of an accretion disk, as measured by a local observer comoving with the fluid, for two perfect fluid singular models with $\lambda = 1/\sqrt{2}$ ($\rho_b = 6$) and $\lambda = 2/\sqrt{5}$ ($\rho_b = 12$). The dotted line corresponds to a disk around a Schwarzschild black hole, while the two dashed lines are for accretion disks in models with purely tangential pressure [8], which are discussed in section III C. (b) Close-up of the flux profiles near the matching radius. Note the discontinuity in the flux, which is caused by the discontinuous behavior of $\omega_{,\rho}$ in equation (58). (c) Profile of the differential luminosity reaching an observer at infinity, $d\mathcal{L}_\infty/d\ln\rho$, for the same models. (d) Close-up of the region near the matching radius.

respect to the radius ρ can be computed from $\mathcal{F}$ by the following relation [20]:

$$\frac{d\mathcal{L}_\infty}{d\ln\rho} = 4\pi\rho\sqrt{-g}E\mathcal{F}. \tag{60}$$

Panels (c) and (d) in Figure 4 show $d\mathcal{L}_\infty/d\ln\rho$ for the two models under consideration. We see that the luminosity behaves in a perfectly convergent fashion as $\rho \to 0$: $d\mathcal{L}_\infty/d\ln\rho \sim \rho^{1-\lambda}$. By integrating this quantity over $\ln\rho$, we can calculate the net luminosity $\mathcal{L}_\infty$ observed at infinity. We have confirmed that this is equal to $\dot{m}c^2$ for the two singular models. That is the disk has 100% efficiency — it converts the entire rest mass energy of the accreting gas into radiation. The dotted lines in the panels indicate the very different behavior of a disk around a Schwarzschild black hole. Since such a disk is truncated at the ISCO, the

luminosity is much less. In this case, we recover the standard result, $\mathcal{L}_\infty = (1 - E_{\rm ISCO})\,\dot{m}c^2 = 0.05719\,\dot{m}c^2$, i.e., an efficiency of 5.719%.

Is it possible to distinguish observationally whether a given accretion system is a black hole or one of the toy singular objects described in this paper? We have seen above that the accretion efficiencies are very different. However, the efficiency is not easily determined via observations since there is no way to obtain an indepedent estimate of the mass accretion rate $\dot{m}$. A more promising avenue is the spectral energy distribution of the disk radiation.

Following standard practice, we assume that each local patch of the disk radiates as a blackbody. Defining a characteristic temperature T_* as follows (where we have included physical units),

$$\sigma T_*^4 \equiv \frac{\dot{m}c^2}{4\pi(GM_T/c^2)^2}, \tag{61}$$

where σ is the Stefan-Boltzmann constant, the local blackbody temperature of the radiation emitted at any radius ρ with flux $\mathcal{F}$ (eq. 58) is given by

$$T_{\rm BB}(\rho) = [\mathcal{F}(\rho)]^{1/4} T_*. \tag{62}$$

This radiation is transformed by gravitational and Doppler redshifts by the time it reaches an observer at infinity and hence appears to have a different temperature. The transformation depends on the orientation of the observer with respect to the disk axis. To avoid getting into too much detail, we simply use a single characteristic redshift z, corresponding to an observer along the disk axis,

$$1 + z(\rho) = [-(g_{tt} + \omega^2 g_{\phi\phi})]^{-1/2}, \tag{63}$$

and assume that the radiation emitted at radius ρ has a temperature at infinity, independent of direction, given by

$$T_\infty(\rho) = T_{\rm BB}(\rho)/(1+z). \tag{64}$$

It is then straightforward to convert the differential luminosity calculated in equation (60) into the spectral luminosity distribution $\mathcal{L}_{\nu,\infty}$ observed at infinity. The result is

$$\nu\mathcal{L}_{\nu,\infty} = \frac{15}{\pi^4}\int_{\rho_{\rm in}}^{\infty}\left(\frac{d\mathcal{L}_\infty}{d\ln\rho}\right)\frac{(1+z)^4(h\nu/kT_*)^4/\mathcal{F}}{\exp[(1+z)h\nu/kT_*\mathcal{F}^{1/4}]-1}\,d\ln\rho. \tag{65}$$

As a check, we have verified numerically that the integral over frequency of the spectral luminosity $L_{\nu,\infty}$ obtained via the above relation is equal to $\dot{m}c^2$ (100% efficiency) for the singular models and equal to $0.05719\dot{m}c^2$ for the Schwarzschild case (5.719% efficiency).

Figure 5 shows spectra corresponding to the same models considered in Figure 4. For a given accretion rate $\dot{m}$, the Schwarzschild black hole model gives a much lower luminosity than the naked singular models. However, as we discussed earlier, this is not observationally testable. More interesting is the fact that the spectra have noticeably different shapes. At low frequencies, all the models have the same spectral shape $\nu L_\nu \sim \nu^{4/3}$, which is the standard result for disk emission from large non-relativistic radii [21]. However, there are dramatic differences at high frequencies.

The emission from a disk around a Schwarzschild black hole cuts off at the ISCO radius $\rho_{\rm ISCO} = 6$. Correspondingly, there is a certain maximum temperature for the emitted radiation, which causes the spectrum to cutoff abruptly at a frequency $h\nu/kT_*$ somewhat below unity. The two perfect fluid singular models, on the other hand, behave very differently. In these models, the disk extends all the way down to $\rho \to 0$. Consequently, the temperature $T_{\rm BB}$ of the emitted radiation rises steadily and diverges as $\rho \to 0$. The emission from all the inner radii combines to produce a power-law spectrum at high frequencies [35]: $\nu\mathcal{L}_{\nu,\infty} \sim \nu^{-8(1-\lambda)/(6\lambda-2)}$.

As Figure 5 shows, the high-frequency power-law segment of the spectrum carries a substantial fraction (more than half) of the total emission from disks around our naked singularity models. The presence of this strong power-law spectrum is thus a characteristic feature of these models which can be used to distinguish them qualitatively from disks around black holes. Several well-known astrophysical black hole candidates are known to have spectra with a strong thermal cutoff, similar to that seen in the dotted line in Figure 5 [22]. These systems show very little power-law emission at high frequencies. In these cases at least we can state with some confidence that the central mass does not have a naked singularity of the sort discussed in this paper.

C. Comparison of the perfect fluid and tangential pressure models

In our previous paper [8], we considered a relatively restricted model in which the fluid in the cloud has non-zero pressure only in the tangential direction. Because of vanishing radial pressure, matching pressure across the boundary radius ρ_b between

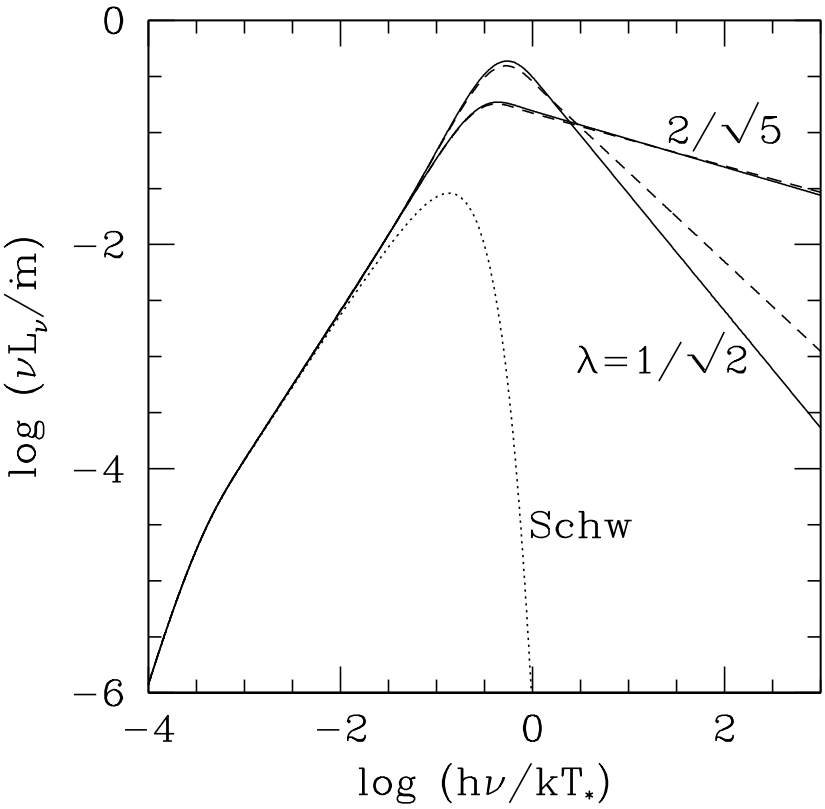


FIG. 5: Spectral luminosity distribution of radiation from the accretion disk models in Figure 4. The dotted line corresponds to a disk around a Schwarzschild black hole, the solid lines correspond to disks around two perfect fluid naked singularity models discussed in this paper, and the dashed lines are for disks around two tangential pressure naked singularity models discussed in [8].

the cloud and the external Schwarzschild spacetime was trivial, and hence the solution was more easily determined. For radii inside the cloud, the metric of the pure tangential pressure model takes the form,

$$ds^2 = -H(\rho)dt^2 + \frac{d\rho^2}{(1-M_0)} + \rho^2 d\Omega^2, \quad \rho \leq \rho_b, \tag{66}$$

with $H(\rho) = (1-M_0)\,(\rho/\rho_b)^{M_0/(1-M_0)}$ and $M_0 = 2M_T/\rho_b$, where M_T is the total gravitational mass of the cloud as measured in the vacuum exterior.

The close similarity of the tangential pressure model and the perfect fluid model described in the present paper is obvious, e.g., compare the above expressions with equations (44) and (36). The constant M_0 in the tangential pressure model plays the role of λ for the perfect fluid case, and in both cases this parameter determines the compactness of the cloud as measured by its dimensionless radius ρ_b/M_T. The limits $M_0 \to 0$ and $\lambda \to 1$ in the two models correspond to infinitely large and dilute clouds that are fully non-relativistic: $\rho_b/M_T \to \infty$. In this limit, the two models are essentially identical. One minor difference between the models occurs in the opposite limit. For the perfect fluid cloud, the most compact configuration we find has $\lambda = 0$, which corresponds to $\rho_b = 4M_T$. In contrast, for the tangential pressure model, the most compact physically valid configuration has $M_0 = 2/3$, which corresponds to $\rho_b = 3M_T$, i.e., a more compact object.

Another difference between the two models is that the tangential pressure cloud has a particularly straightforward metric in which $g_{tt} = H(\rho)$ varies with radius as a simple power-law. Therefore, all quantities behave as power-laws and the analysis is easy. In the case of the perfect fluid model, the extra matching condition on the pressure at $\rho = \rho_b$ results in the metric coefficient g_{tt} involving two power-laws. The term involving the coefficient A in equation (44) dominates as $\rho \to 0$ and behaves just like the lone power-law term in the tangential pressure cloud case. The second term involving B is required in order to satisfy the pressure boundary condition and plays a role only as ρ approaches ρ_b. This term causes various quantities like E, L, ω, etc. to deviate from perfect power-law behavior as $\rho \to \rho_b$ (see Figs. 1–4).

As far as observables are concerned the two models behave quite similarly. In Figs. 4 and 5, the two perfect fluid models with $\lambda = 1/\sqrt{2}$ and $2/\sqrt{5}$ have boundaries at $\rho_b = 6$ and 12, respectively, and their properties are shown by the solid lines. For

comparison, the dashed lines show results for two tangential pressure models with $M_0 = 1/3$ and $1/6$ which have boundaries at the same radii, $\rho_b = 6,\ 12$. While the agreement between the two sets of models is not perfect, as is to be expected since the models are different, we see very good qualitative agreement. In particular, note that, just as in the perfect fluid models, the tangential pressure models too produce a strong power-law high energy tail in the spectra of their accretion disks (Fig. 5), which may be used to distinguish these models from disks around a Schwarzschild black hole (dotted line).

D. Comparison with the Newtonian singular isothermal sphere

A simple and commonly used model in astrophysics is the singular isothermal sphere. This is a spherically symmetric self-gravitating object with an equation of state $p = \epsilon c_s^2$, where p is the pressure, ϵ is the density (this is usually called ρ but we use ϵ here since we have already defined ρ to be the radius), and c_s is the isothermal sound speed. The model satisfies the condition of hydrostatic equilibrium under the action of Newtonian gravity. The solution is

$$\epsilon(\rho) = \frac{c_s^2}{2\pi G\rho^2}, \qquad p(\rho) = \frac{c_s^4}{2\pi G\rho^2}, \qquad M(\rho) = \frac{2c_s^2\rho}{G}, \tag{67}$$

where $M(\rho)$ is the mass interior to radius ρ. The variations of ϵ, p and M with ρ are very reminiscent of the variation of ϵ, p and F in the perfect fluid relativistic cloud model described earlier.

One deficiency of the basic singular isothermal sphere model is that it extends to infinite radius, where the mass is infinite. In order to obtain an object with a finite radius, one needs to change the equation of state such that the pressure goes to zero at a finite density. This is easily arranged as follows:

$$\epsilon(\rho) = \frac{c_s^2}{2\pi G\rho^2} = \frac{\rho_b^2}{\rho^2}\epsilon_b, \qquad \epsilon_b \equiv \frac{c_s^2}{2\pi G\rho_b^2}, \qquad p(\rho) = c_s^2(\epsilon - \epsilon_b), \qquad M(\rho) = 4\pi\epsilon_b r_b^2\rho, \qquad \rho \le \rho_b, \tag{68}$$

where ρ_b is the radius of the boundary and ϵ_b is the density at that radius.

Circular orbits inside a singular isothermal sphere behave very simply, with velocity and angular momentum given by

$$v_{\rm circ} = \sqrt{c_s}\,\rho = \text{const}, \qquad L = \sqrt{2}\,c_s\rho, \qquad \rho \le \rho_b. \tag{69}$$

The constancy of $v_{\rm circ}$ is the chief attraction of the singular isothermal sphere. It provides a simple way of reproducing the observed flat rotation curves of galaxies. The scaling of L with ρ in the singular isothermal sphere is exactly the same as the variation of L with ρ in the perfect fluid relativistic cloud. At first sight it appears that the flat rotation curve property is not reproduced in the relativistic model. For example, $\omega\rho$ scales as $\rho^{1-\lambda}$. However, note that ω is defined as $d\phi/dt$, where t is the time measured at infinity. The appropriate quantity to consider is $d\phi/dt_{\rm loc}$, where $t_{\rm loc}$ is time measured by a local ZAMO (Zero Angular Momentum Observer) at radius ρ. The two times are related by a factor of $[H(\rho)]^{1/2}$ which varies as $A\rho^{1-\lambda}$ in the limit $\rho \to 0$. Thus, for ZAMOs, the rotation velocity is indeed independent of radius in the deep interior of the cloud. (Close to the boundary, there are small deviations because of the term involving B in $H(\rho)$).

Consider next the energy of circular orbits in the singular isothermal sphere model. If we include the rest mass energy and add to it the orbital kinetic energy and the potential energy, then a Newtonian calculation gives for the energy of a particle of unit mass

$$E_{\rm circ} = 1 - \frac{c_s^2}{c^2}\left(1 + 2\ln\frac{\rho_b}{\rho}\right), \qquad \rho \le \rho_b. \tag{70}$$

The weak logarithmic divergence at small radii is rarely a problem since we generally have $c_s \ll c$. Nevertheless, the presence of the logarithm implies that, in principle, at a sufficiently small radius, the Newtonian model predicts a *negative* total energy for the particle. This is clearly unphysical.

It is reassuring that the logarithmic divergence is not present in our relativistic cloud models. Both the pefect fluid model and the tangential pressure model have E varying as a power-law with radius: $E \sim \rho^{1-\lambda}$ for the perfect fluid case and $E \sim \rho^{M_0/2(1-M_0)}$ for the tangential pressure case. In both cases, E asymptotes precisely to zero as $\rho \to 0$ and does not go negative anywhere. Effectively, the relativistic models, being more self-consistent, regularize the logarithm of the Newtonian model by replacing it with a power-law. The index of the power-law is nearly 0 in the Newtonian limit but becomes as large as unity for the maximally compact configuration, viz., $\lambda = 1$ and $M_0 = 2/3$ for the perfect fluid and tangential pressure models, respectively.

E. Other models

As we have seen above, the perfect fluid relativistic model described in this paper is equivalent to the Newtonian singular isothermal sphere model used in astrophysics. The relativistic generalization was obtained by assuming that the energy density

$\epsilon(\rho)$ in the relativistic model has the same functional form as $\epsilon(\rho)$ in the Newtonian model (compare eqs. 37 and 68), and then solving for the pressure p and the spacetime metric. This procedure can be followed with any other trial model of $\epsilon(\rho)$ of interest.

One simple example is to consider a superposition of the toy perfect fluid model described in this paper with the well known constant density Schwarzschild interior. The density profile then takes the form

$$\epsilon = \frac{M_0}{\rho^2} + M_1, \tag{71}$$

which corresponds to

$$F(\rho) = M_0\rho + M_1\rho^3/3. \tag{72}$$

The density in this model approaches the singular interior of our perfect fluid model as $\rho \to 0$ but resembles a constant density interior with $\epsilon = M_1$ as $\rho \to \rho_b$. It turns out that the TOV equation can be explicitly integrated in this case, though the expression for p is fairly complicated and involves hypergeometric functions.

Other examples of more interest to astrophysics could be similarly considered. One natural generalization of the singular isothermal sphere is the Jaffe density profile [23],

$$\epsilon = \frac{M_0 r_0}{\rho^2(\rho_0 + \rho)^2}, \tag{73}$$

where M_0 is a constant and ρ_0 describes the characteristic radius of the object. This density profile corresponds to

$$F(\rho) = \frac{M_0\rho}{(\rho_0 + \rho)}. \tag{74}$$

The Jaffe model behaves just like the singular isothermal sphere as $\rho \to 0$, yet it has a finite total mass given by M_0 and hence does not need to be artifically truncated as we had to in the case of the singular isothermal sphere. The Jaffe model is a special case of a more general class of models, the Dehnen density profile [24],

$$\epsilon = \frac{(3-\gamma)M_0\rho_0}{\rho^\gamma(\rho + \rho_0)^{4-\gamma}}. \tag{75}$$

The Jaffe profile corresponds to $\gamma = 2$, while the case with $\gamma = 1$ is known as the Hernquist model [25]. The Dehnen profile implies a mass function

$$F(\rho) = M_0\left(\frac{\rho}{\rho_0 + \rho}\right)^{3-\gamma}. \tag{76}$$

Finally, we could also consider the Navarro-Frenk-White (NFW) profile [26], which is given by

$$\epsilon = \frac{M_0}{\rho(\rho_0 + \rho)^2}, \tag{77}$$

where again M_0 is a constant. This model has a logarithmically diverging mass as $\rho \to \infty$, and is thus a little less attractive.

It is not easy to solve the TOV equations for the pressure p and the spacetime metric of any of the above models analytically. However, numerical solutions are easily obtained. Note that all these popular models technically have naked singularities at their centers. Obtaining relativistic generalizations along the lines followed in this paper would be worthwhile.

IV. CONCLUDING REMARKS

In the present paper we considered a self-bound spherical cloud of perfect fluid and derived static non-vacuum solutions of the Einstein equations which posseses a central naked singularity. We showed that these solutions could be obtained asymptotically as the final result of the slow collapse of a massive matter cloud. The solutions described here closely parallel those we obtained in [8] for a fluid with pure tangential pressure.

We studied the properties of steady thermal accretion disks in our naked singularity spacetimes. Focusing on those models that have a disk extending continuously from a large radius ρ down to $\rho \to 0$, i.e., models with $\lambda \geq 1/\sqrt{2}$ for the perfect fluid case and $M_0 \leq 1/3$ for the tangential pressure case, we showed that accretion disk spectra would consist of a multi-temperature blackbody at low frequencies joining smoothly to a power-law at high frequencies. Notably, the disk luminosity would be dominated by the high-energy tail, which is a characteristic feature of these models. The spectrum of an equivalent accretion

disk around a black hole would have only the low-frequency multi-temperature blackbody component and would be missing the high frequency tail (or at best have a weak tail).

Accretion disks around astrophysical black hole candidates do show power-law tails, but these are usually interpreted as coronal emission from hot gas above the disk. In those cases where the disk emission is definitely thermal, e.g., in the so-called Thermal State of accreting stellar-mass black holes [27], the spectrum is invariably dominated by the low-frequency multi-temperature emission and the power-law tail tends to be quite weak. A number of stellar-mass black holes have been observed in the Thermal State [28]. In the case of these systems at least we may conclude that the central compact objects are not naked singularities of the type discussed in the present paper; the objects are presumably true black holes. However, it is not possible to state anything with certainty in the case of other black hole candidates that have not been observed in the Thermal State.

The existence of horizons in stellar mass astrophysical sources has been a matter of discussion in recent years (see for example [1], [29] and references therein). Some observations suggest that the departure of such objects from black holes must be very small [30]. All the same, when it comes to more massive sources, excess luminosity from Ultra Luminous X-ray Sources cannot at present be explained fully by the usual black hole accretion disk models and seem to require the existence of as yet undiscovered intermediate mass black holes [31].

Since there is a strong thermal cutoff at high frequencies present in the spectrum of the black hole models while it is absent in the perfect fluid naked singularity models studied here, this strenghtens the argument that the astrophysical sources that exhibit the same behaviour would be black holes. On the other hand, ultra luminous sources exist in the universe and at present it is not clear if it will be possible to fit all the observations within the black hole paradigm. It is possible that different kinds of sources exist in nature, besides black holes, stars and neutron stars. These could be of the singular type discussed here or could be regular objects composed of ordinary or exotic matter. All these could possibly form from collapse processes as described here and they would have their distinctive observational features (see for example [33]). In such a scenario, the comparison and models such as the ones discussed here may be useful to understand better and analyze future observations.

For the toy models presented here we found that the radiant energy flux and the spectral energy distribution are much greater as compared to a black hole of the same mass, and therefore we obtained indications that if some sources of similar kind do exist in the universe it might be possible to distinguish them observationally from black holes.

We also found here that the qualitative features described in [8] are preserved when we consider perfect fluid sources, instead of sources sustained only by tangential stresses. We can therefore conjecture that the increased flux and luminosity may be a generic feature of any source with a singularity at the center where the accretion disk can in principle extend until $r = 0$. As it is known, perfect fluids are important in the context of astrophysics as they can be used to model many sources and objects of astrophysical relevance. Of course, different matter models will imply different luminosity spectrums that might or might not eventually be distinguished from one another.

Finally, we note that these models require a certain fine tuning since all the collapsing shells must have the right velocity so that the effective potential leads asymptotically to $\dot{R} = \ddot{R} = 0$. Nevertheless the class of static final configurations can be understood in the sense of an idealized approximation for a slowly evolving cloud with small velocities. In this sense these scenarios appear to be generic as they approximate a wide variety of slowly evolving matter clouds.

---

[1] R. Narayan and J. E. McClintock, New Astron. Rev. **51**, 733-751 (2008); and references therein.

[2] P. S. Joshi and D. Malafarina, Int. J. Mod. Phys. D **20**, 2641 (2011); and references therein.

[3] B. Freedman and L. D. McLerran, Phys. Rev. D **17**, 11091122 (1978); M. Colpi, S. L. Shapiro and I. Wasserman, Phys. Rev. Lett. **57**, 24852488 (1986); D. F. Torres, S. Capozziello and G. Lambiase, Phys. Rev. D **62** (10), 104012 (2000); P. O. Mazur and E. Mottola, arXiv:0109035 [gr-qc]; D. F. Torres, Nucl. Phys. B **626**, 377 (2002); P. Jaikumar, S. Reddy and A. Steiner, Phys. Rev. Lett. **96**, 041101 (2006); M. Visser, C. Barcelo, S. Liberati and S. Sonego, arXiv:0902.0346 [gr-qc]; F. E. Schunck and E. W. Mielke, Class. Quantum Grav. **20**, 301 (2003).

[4] A. N. Chowdhury, M. Patil, D. Malafarina and P. S. Joshi, Phys. Rev. D **85**, 104031 (2012); D. Pugliese, H. Quevedo and R. Runi, Phys. Rev. D **83** 024021 (2011); D. Pugliese, H. Quevedo and R. Runi, Phys. Rev. D **83** 104052 (2011); P. Pradhan and P. Majumdar, Phys. Lett. A **375**, 474 (2011).

[5] C. Bambi, Mod. Phys. Lett. A **26**, 2453-2468 (2011); C. Bambi, K. Freese, T. Harada, R. Takahashi and N. Yoshida, Phys. Rev. D **80**, 104023 (2009); Z. Stuchlik and J. Schee, Class. Quantum Grav. **27**, 215017 (2010); D. Pugliese, H. Quevedo and R. Runi, Phys. Rev. D **84**, 044030 (2011);

[6] Z. Kovacs and T. Harko, Phys. Rev. D **82**, 124047 (2010).

[7] E. G. Gimon and P. Horava, Phys. Lett. B **672**, 299 (2009).

[8] P. S. Joshi, D. Malafarina and R. Narayan, Class. Quantum Grav. **28**, 235018 (2011).

[9] R Giambó, Class. Quantum Grav. **22**, 2295 (2005); W. Israel, Nuvo Cemento B **44**, 1 (1966); W. Israel, Nuvo Cemento B **48**, 463 (1966).

[10] P. S. Joshi and R. V. Saraykar, Int. J of Mod Phys. **22**, 1350027 (2013).

[11] P. S. Joshi and I. H. Dwivedi, Phys. Rev. D **47**, 5357 (1993); B. Waugh and K. Lake, Phys. Rev. D **38**, 1315 (1988); R. P. A. C. Newman, Class. Quantum Grav. **3**, 527 (1986); D. Christodoulou, Commun. Math. Phys. **93**, 171 (1984); D. M. Eardley and L. Smarr, Phys. Rev. D **19**, 2239 (1979).

[12] T. A. Madhav, R. Goswami and P. S. Joshi, Phys Rev D **72**, 084029 (2005); A. Mahajan, T. Harada, P. S. Joshi and K. I. Nakao, Prog. Theor. Phys. **118**, 865-878 (2007).
[13] K. Lake, Phys. Rev. D **67**, 104015 (2003).
[14] P. S. Joshi and I. H. Dwivedi, Class. Quantum Grav. **16**, 41 (1999).
[15] M. S. R. Delgaty and K. Lake, Comput. Phys. Commun. **115**, 395 (1998).
[16] D. Martin and M. Visser, Phys. Rev. D **69**, 104028 (2004).
[17] R. Wald, *General Relativity*, University Of Chicago Press, p. 125 (1984).
[18] R. C. Tolman, Phys. Rev. **55**, 364 (1939).
[19] D. Bini, D. Gregoris, K. Rosquist and S. Succi, Gen. Rel. Grav. **44** (10), 2669 (2012).
[20] D. Novikov and K. S. Thorne in *Black Holes*, ed. C. DeWitt and B. S. DeWitt, New York: Gordon and Breach, p. 343 (1973); D. N. Page and K. S. Thorne, Astrophys. J. **191**, 499 (1974).
[21] J. Frank, A. King and D. J. Raine, *Accretion Power in Astrophysics*, Third edition, Cambridge Univ. Press (2002).
[22] S. W. Davis, C. Done and O. Blaes, Astrophys. J. **647**, 525 (2006); L. Gou et al., Astrophys. J. **718**, L122 (2010); J. F. Steiner et al., Mon. Not. Royal Astr. Soc. **416**, 941 (2011).
[23] W. Jaffe, Mon. Not. Royal Astr. Soc. **202**, 995 (1983).
[24] W. Dehnen, Mon. Not. Royal Astr. Soc. **265**, 250 (1993).
[25] L. Hernquist, Astrophys. J. **356**, 359 (1990).
[26] J. F. Navarro, C. S. Frenk and S. D. M. White, Astrophys. J. **463**, 563 (1996).
[27] R. A. Remillard and J. E. McClintock, Ann. Rev. Astron. Astrophys. **44**, 49 (2006).
[28] J. E. McClintock, R. Narayan and J. F. Steiner, arXiv astro-ph:1303.1583.
[29] E. Maoz, Astrophys. J. **494**, L181 (1998); A. E. Broderick, A. Loeb and R. Narayan, Astrophys. J. **701**, 1357 (2009); M. A. Abramowicz, W. Kluzniak and J. P. Lasota, Astron. Astrophys. **396**, L31 (2002); C. Bambi, arXiv:1205.4640 [gr-qc].
[30] S. S. Doeleman et.al. Nature, **455**, 78 (2008).
[31] J. M. Miller, A. C. Fabian and M. C. Miller, Astrophys. J. **614**, L117 (2004).
[32] Critical Collapse of Einstein Cluster Ashutosh Mahajan, Tomohiro Harada, Pankaj S. Joshi, Ken-ichi Nakao, Prog. Theor. Phys. **118**, 865-878 (2007).
[33] C. Bambi and D. Malafarina, arXiv:1307.2106; P. S. Joshi and D. Malafarina, *Compact objects from gravitational collapse: an analytical toy model* (in progress).
[34] Of course as the particles approach the center friction and viscosity will play an increasingly important role thus deviating the behaviour from that of a classical accretion disk [19]. Nevertheless we can assume that until a certain radius the approximations made here are satisfied.
[35] Note that models with $\lambda < 1/3$ do not have a high energy power-law tail. These models belong to the class of models with $\lambda < 1/\sqrt{2}$ which we have decided to ignore in this paper since their disks have a gap between the ISCO of the external Schwarzschild spacetime and the surface of the cloud.